Electronic transport in dense fully ionized hydrogen

H. Minoo and C. Deutsch
Laboratoire de Physique des Plasmas, Université Paris XI, Bâtiment 212, Orsay, 91405, France*

J. P. Hansen
Laboratoire de Physique Théorique des Liquides,† Université Paris VI, 4 Place Jussieu, 75005 Paris, France
(Received 22 March 1976)

Electronic transport is considered in dense fully ionized hydrogen. The equivalence of the Boltzmann-Ziman approach with the more deductive Kubo formalism for weak electron-ion interactions is established. The ionic structure factors obtained from recent and improved Monte Carlo simulation of the classical one-component plasma are used to obtain the linear time-independent transport coefficients. The effects of inelastic electron scattering from the ionic density fluctuations are taken into account. The electrical and thermal conductivities, the conductive opacity, the bulk viscosity, and the thermoelectric power at different densities and temperatures are tabulated. These results are compared with previous calculations.

I. INTRODUCTION

We are concerned here with the problem of calculating the electronic transport coefficients of dense conducting fluids consisting solely of massive point ions and a neutralizing background of fully degenerate weakly interacting electrons. When the electron mean free path is larger than the ionic binary correlation length, the nearly-free-electron (NFE) approximation applies, and the various time-independent transport quantities may be easily obtained within the framework of the standard Lorentz model, where the electrons are elastically deflected at the surface of the Fermi sphere by the ion density fluctuations. Usually, it is sufficient to consider the weak electron-ion interaction in the Born approximation, while the strong ionic equilibrium correlations are taken care of through the binary structure factor $S(k)$. This is essentially the basic content of the well-known Boltzmann-Ziman[1] formulation of electronic transport, extensively used in liquid-metal physics. It has been extended[2] to the critical domain of alkali-metal vapors with the use of a hydrodynamic approximation for the generalized structure factor $S(k,\omega)$ to explain the sudden breakdown of the metallic conductivity in the vicinity of the liquid-vapor critical point. The same approach has also been recently applied[3] to the electric resistivity of fully ionized liquid metals with hard-sphere ionic structure factors.

In this work, we address ourselves to an extension to other electronic transport coefficients, such as thermal conductivity, conductive opacity, thermoelectric power, and bulk viscosity. Our calculations make use of the ionic structure factors obtained by one of us[4] from Monte Carlo simulations for the equilibrium properties of the one-component plasma (OCP) model in a neutralizing background, in terms of the dimensionless classical plasma parameter $\Gamma = \beta(Ze)^2/r_i$, where $r_i = (\frac{4}{3}\pi n_i)^{-1/3}$ is the ion sphere radius, $\beta = (k_B T)^{-1}$, and n_i is the ionic number density.

The present transport calculations are basically motivated by their relevance to the computation of the physical properties of the deep interior of giant planets such as Jupiter and of the white-dwarf stars. The connection with laboratory physics lies in our estimate of the electronic thermal conductivity, which is essential to the energy balance of highly compressed deuterium plasma[5] (see Fig. 1), obtained from laser compression in order to reach charge densities and temperatures capable of sustaining nuclear fusion reactions.

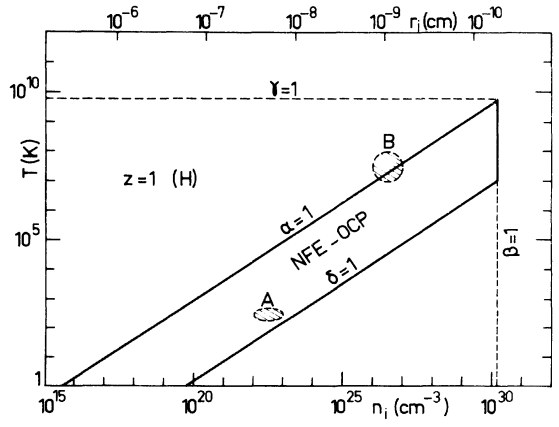

FIG. 1. Region of simultaneous validity of both NFE and OCP models. $\alpha \equiv k_B T/\epsilon_F$, $\beta \equiv \epsilon_F/m_e c^2$, $\gamma \equiv k_B T/m_e c^2$, $\delta \equiv \Lambda/r_i$. Subregions A and B correspond to initial and final states of systems under laser-driven fusion conditions.

The application to dense alkali vapors (Na, Cs, etc.) in the critical regime, or in the electrode region of some discharges (cathode spots in arcs and sparks, exploding wires, etc.) will be given further attention in a subsequent work.

The paper is organized as follows: In Sec. II the conditions of validity of the NFE approximation are explicitly given. The Ziman formulation is detailed in Sec. III for the various linear electronic transport coefficients, and the equivalence of the Boltzmann-Ziman approach with the more deductive Kubo formulation for weak electron-ion interactions is also pointed out. The choices of the effective electron-ion interaction $U(k)$ and of the ionic structure factor are considered in Sec. IV. The numerical results are presented in Sec. V and discussed in Sec. VI.

II. NFE MODEL FOR ELECTRON TRANSPORT

In order to be able to use the NFE model one assumes the following:

(a) The temperature of the system is such that the electron gas remains degenerate:

$$\alpha \equiv k_B T/\epsilon_F \ll 1 \quad \text{or} \quad T(\mathrm{K}) \ll 6\times 10^5/r_s^2 , \tag{1}$$

where r_s is defined as usual, $r_s = r_e/a_0$, and $r_e = (3/4\pi n_e)^{1/3}$ is the radius of a sphere that contains one electron, a_0 is the first Bohr radius, and $\epsilon_F = \hbar^2(3\pi^2 n_e)^{2/3}/2m_e$ is the Fermi energy.

(b) The electron density is not too large, so that the electrons can be treated nonrelativistically:

$$\beta \equiv \epsilon_F/m_e c^2 \ll 1 \quad \text{or} \quad n_e \ll 1.66\times 10^{30}\ \mathrm{cm}^{-3} . \tag{2}$$

(c) The Lorentz gas model is applicable, i.e., the electrons interact only with ions. In a highly degenerate system the electron-electron interaction can be neglected as a result of the exclusion principle. At higher temperatures the electron-electron interaction could become important.[6]

(d) The electron scattering cross section from the ionic system can be calculated in the first Born approximation. This approximation is adequate wherever[7]

$$r_{ei} \lesssim \lambda\!\!\!^{-}_{ei} ,$$

where

$$r_{ei} = Ze^2/\epsilon_F \quad \text{and} \quad \lambda\!\!\!^{-}_{ei} = \hbar/(2m_e\epsilon_F)^{1/2} .$$

The critical density for the validity of this approximation is then defined by

$$r_s \lesssim 1/Z . \tag{3}$$

(e) The mean free path of the conduction electrons λ_e is sufficiently large,

$$\frac{\lambda_e}{r_i} > 1 \quad \text{or} \quad 2\pi r_s \frac{\sigma_e}{\sigma_0}\left(\frac{2\pi}{3Z}\right)^{1/3} > 1 , \tag{4}$$

where σ_e is the electrical conductivity and $\sigma_0 = e^2/a_0\hbar$, viewed as the atomic unit of the electrical conductivity,[3] has the practical value of $4.6\times 10^4\ \Omega^{-1}\,\mathrm{cm}^{-1}$. The condition on λ_e implies that the conductivity of the system is sufficiently high such that

$$\sigma_e > 5.72\times 10^3 Z^{1/3}/r_s \ \ \Omega^{-1}\,\mathrm{cm}^{-1} . \tag{5}$$

III. TRANSPORT COEFFICIENTS

A. Basic considerations

We pay special attention to the simple situation with completely degenerate electrons while the ions remain classical. The interest of such a model for the computation of thermal and electric properties in dense and high-temperature plasmas has long been recognized.[3,8] However, two distinct approaches, both using the Lorentz model of weakly interacting electronic plane waves elastically diffused by the classical ions, are considered without any apparent appreciation of their relative merits and possible connections between them. The first one[8] relies on the deductive Kubo formalism[9] (see Appendix D for an explicit derivation), while the second one (Ref. 3 and references cited therein) makes use of the Boltzmann equation for the electronic transport of liquid metals.[1] Our purpose is to emphasize that both methods produce identical results for the electronic thermal conductivity and the other related linear electric transport coefficients, provided that the above-mentioned requirements for the use of the Lorentz model are satisfied. To save space, let us start from the usual Ziman expression for the thermal conductivity K_e^0,[10] restricted to the elastic approximation fulfilling the Wiedemann-Franz relation,

$$\rho K_e^0/T = \tfrac{1}{3}\pi^2(k_B/e)^2 , \tag{6}$$

where ρ is the standard Ziman expression

$$\rho = \frac{m_e^2}{12\pi^3\hbar^3 e^3 n_e}\int_0^{2k_F} dk\, k^3 \left|U(k)\right|^2 S(k) \tag{7}$$

for the electron resistivity given explicitly in terms of the Coulomb electron-ion interaction $4\pi n_e e^2/k^2$ with the dielectric constant put equal to 1.[8]

Vieillefosse and Hansen[11] obtained an analytical expression for the ionic structure factor $S(k)$ in the long-wavelength limit. Their result is

$$S(q) = \frac{q^2}{3\Gamma + q^2(K_T^0/K_T)} , \tag{8}$$

where $q = kr_i$ is the reduced wave number, $K_T = (1/n_i)(\partial n_i/\partial P)_T$ is the isothermal compressibility of the OCP, and $K_T^0 = \beta/n_i$ is the ideal-gas compressibility. K_T can be obtained from Eqs. (11)

and (20) of Ref. 4. The usual high-temperature (Debye) approximation is recovered for $K_T = K_T^0$. Collecting Eqs. (6)–(8) one readily obtains

$$K_e = \frac{(2\pi\hbar)^3 n_i}{16 m_e^2 e^4} \frac{\alpha k_B^2 T}{\ln[1+(4\alpha q_F^2/3\Gamma)]}, \tag{9}$$

where $q_F = k_F r_i$, $k_F = (\frac{9}{4}\pi)^{1/3}/r_e$, and $\alpha = K_T^0/K_T$. Equation (9) is nothing but the result obtained from the Chester-Thellung-Hubbard formalism detailed in Appendix D.

Finally, it is worth pointing out that the above result is a special case[12] of the identity of the Kubo and Boltzmann formalisms when the interaction is weak, or possibly strong but still localized.

B. Linear electronic transport coefficients

In the framework of the Boltzmann-Ziman formulation of electronic transport, all linear time-independent transport coefficients are essentially determined by the static structure factor of the ions $S(k)$ and the matrix element of the screened electron-ion interaction $U(k)$, as can be seen from the following expressions.

1. Electrical conductivity

The electrical conductivity is given by

$$\sigma_e = n_e e^2 \tau_\sigma / m_e , \tag{10}$$

with $\tau_\sigma = \lambda_e / v_F$, where v_F is the Fermi velocity, τ_σ is the collision time, and λ_e is obtained from

$$\lambda_e^{-1} = 2\pi n_i \int_0^{2\pi} (1-\cos\theta) I(\theta) \sin\theta \, d\theta . \tag{11}$$

In this formula $I(\theta)$ is the differential scattering cross section of each ion and is to be calculated in the first Born approximation. As originally shown by Ziman,[1] the electrical conductivity σ_e, based on these assumptions, can be written in the following form:

$$\sigma_e^{-1} = \frac{12\pi}{\hbar e^2 v_F^2 n_i} \int_0^1 \left| U\left(\frac{k}{2k_F}\right)\right|^2 S\left(\frac{k}{2k_F}\right)\left(\frac{k}{2k_F}\right)^3 d\left(\frac{k}{2k_F}\right). \tag{12}$$

In order to avoid the repetition of lengthy expressions, it is useful to introduce the following notation:

$$\langle f(x)\rangle \equiv \int_0^1 dx\, x^3 |U(x)|^2 f(x); \tag{13}$$

with this notation Eq. (12) takes the form

$$\sigma_e^{-1} = (12\pi/\hbar e^2 v_F^2 n_i)\langle S(x)\rangle , \tag{14}$$

where $x \equiv k/2k_F$.

2. Thermal conductivity and conductive opacity

The electronic thermal conductivity K_e^0 is related to the electrical conductivity by the Wiedemann-Franz law

$$K_e^0 = L_0 T \sigma_e , \tag{15}$$

where the Lorenz number L_0 has the value

$$L_0 = \tfrac{1}{3}\pi^2 (k_B/e)^2 . \tag{16}$$

As Rice[10] has pointed out, the inelastic scattering of electrons from ionic density fluctuations could modify the Lorenz ratio. Taking into account this effect, the corrected thermal conductivity K_e may be written in the following form:

$$K_e = K_e^0/(1+\alpha_1), \tag{17}$$

with

$$\alpha_1 \simeq (6/\pi^2) y \langle 1 - \tfrac{2}{3}x^2\rangle / \langle S(x)\rangle \tag{18}$$

and

$$y = \hbar^2 k_F^2 / 2 M_i k_B T, \quad x \equiv k/2k_F .$$

M_i is the ionic mass and the angular brackets are defined in (13).

A useful coefficient, which plays an important role in the energy transport formulation of the stellar interior and particularly white-dwarf stars, is the conductive opacity K_c. It is connected, as usual, to the thermal conductivity by the following relation[13]:

$$K_c = \tfrac{16}{3} N_0 a T^3 / M_i n_i K_e , \tag{19}$$

where N_0 is Avogadro's number and a the Stefan-Boltzmann constant.

3. Electronic bulk viscosity

The electronic bulk viscosity η_e is given by

$$\eta_e = \tfrac{2}{5} n_e \epsilon_F \tau_\eta , \tag{20}$$

where τ_η is, in general, different from τ_σ of Eq. (10). Following Baym[14] we write the ratio τ_σ/τ_η as

$$\frac{\tau_\sigma}{\tau_\eta} = \frac{2\epsilon_F m_e \sigma_e}{5 e^2 \eta_e} = \frac{3\langle (1-x^2) S(x)\rangle}{\langle S(x)\rangle} . \tag{21}$$

The electronic bulk viscosity is then obtained from this equation by inserting σ_e from formula (14),

$$\eta_e^{-1} = \frac{45\langle (1-x^2) S(x)\rangle}{\hbar \epsilon_F^2 n_i} . \tag{22}$$

4. Thermoelectric power and the Hall coefficient

The thermoelectric power Q is represented through the dimensionless parameter ξ,

$$\xi = \frac{k_F}{2\sigma_e}\left(\frac{\partial \sigma_e(k)}{\partial k}\right)_F , \tag{23}$$

by

$$Q = (\pi^2 k_B^2 T/3e\epsilon_F)\xi. \tag{24}$$

From Eqs. (23) and (14) it follows that[15]

$$\xi = 3 - \frac{S(2k_F)\,|U(2k_F)|^2}{2\langle S(x)\rangle}. \tag{25}$$

When the Fermi surface is not distorted and remains spherical, the Hall coefficient R and the Hall mobility μ are given by

$$R = 1/en_e, \quad \mu = |R|\sigma_e. \tag{26}$$

IV. CHOICE OF $S(k)$ AND $U(k)$

A. Structure factor

As can be seen from Sec. III, in order to evaluate the transport coefficients at different temperatures, in the framework of the NFE model, it is necessary that the structure factor provide this functional dependence in T. In their calculation of the electronic conductivity in fully ionized liquid metals, Stevenson and Ashcroft[3] used the structure factor appropriate for a fluid of hard spheres in the Percus-Yevick approximation[16] (Appendix B). Although this choice may be adequate at the liquid densities, its use is in general unsatisfactory for the following reasons:

(a) This procedure requires an independent determination of the temperature scale, since hard-sphere properties depend only on density, and one is led to derive independently the temperature dependence of the packing fraction $y(T)$, where

$$y = \tfrac{1}{6}\pi(2r_h)^3 n_i = (r_h/r_i)^3,$$

and r_h is the hard-sphere radius. Although $y(T)$ can be obtained from the slope of the curve of the effective ion-ion interaction energy,[3] it is assumed that $y(T)$ decreases on heating as $(T)^{-\nu}$, where ν is an adjustable parameter.[15]

(b) This variable parameter ν is usually adjusted to fit the experimental results.

(c) Its range of applicability is limited to the fluid densities such that $r_h < r_i < 10r_h$, as is shown in Fig. 9; this is discussed in more detail in Appendix B.

We propose instead to choose, for the ionic structure factor, the structure factor of the classical one-component plasma (OCP), i.e., a system of point charges in a uniform background of conduction electrons. The radial distribution function of this system has been recently determined very accurately by Monte Carlo simulations[4] over an extensive range of thermodynamic states. In Appendix A we show how the structure factor can be extracted from the Monte Carlo data with a very high degree of accuracy. The advantages of this procedure are that it leaves no adjustable parameter, it provides explicitly the temperature dependence of the transport coefficients, and the calculations can be extended to a larger density range, i.e., to the region where $r_i < r_h$. The comparison

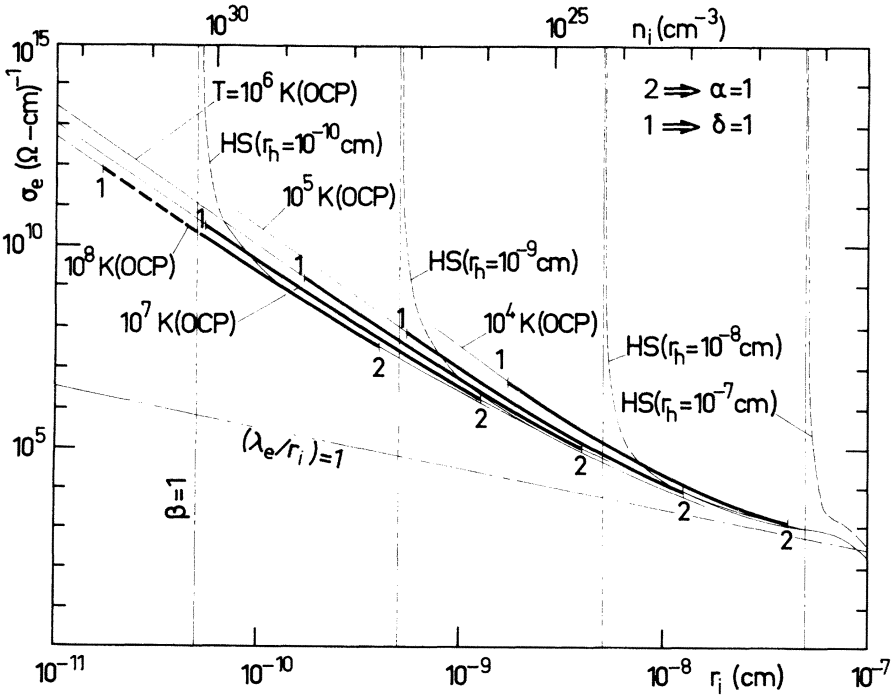

FIG. 2. Electrical conductivity σ_e of hydrogen at different temperatures and densities, with $U(k)$ obtained from expressions (C5) and (C7). Curve OCP: $S(k)$ from OCP. In each curve points 1 and 2 correspond to the conditions $\delta = 1$ and $\alpha = 1$, respectively. Curve HS: $S(k)$ obtained from hard-sphere model. r_h is the hard-sphere radius and λ_e the mean free path of the conduction electrons.

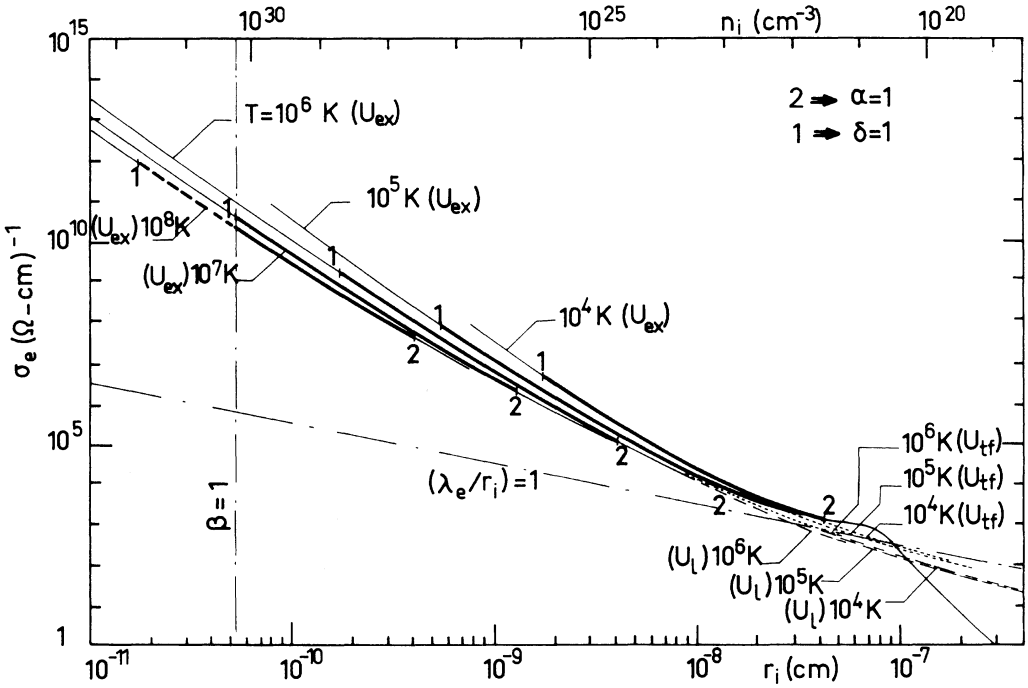

FIG. 3. Electrical conductivity with different $U(k)$ and with $S(k)$ from OCP. Curve U_{ex}: $U(k)$ for the dielectric function, taking into account the exchange and correlation corrections. Curve U_l: $U(k)$ for the Lindhard function. Curve U_{TF}: $U(k)$ for the Thomas-Fermi approximation.

between results obtained with the structure factors of the OCP and of hard-sphere models is made in Fig. 2, where the electrical conductivity of hydrogen at different densities and temperatures is plotted. σ_e was obtained from (14) with $U(k)$ from expressions (C5) and (C7). Curves OCP and HS correspond to $S(k)$ from, respectively, the OCP and hard-sphere models. In these calculations the hard-sphere radius r_h varied from 10^{-10} to 10^{-8} cm. As can be seen from Fig. 2, at a given r_h, which may be viewed as at constant temperature, the use of $S(k)$ from the hard-sphere model limits the calculations to $r_i > r_h$, and as r_i approaches r_h the electrical conductivity diverges, which is not physically satisfactory.

B. Pseudopotential

The choice of $U(k)$ is based on pseudopotential theory, and a brief discussion of the scattering potential and the dielectric constant is given in Appendix C. Figure 3 shows the electrical conductivity obtained with different $U(k)$ and with $S(k)$ from the OCP. Curves U_{TF}, U_l, and U_{ex} correspond, respectively, to the expressions (C4), (C5), and (C7) for the dielectric function. As can be seen from Fig. 3, when $r_s < 1$, the different expressions for $U(k)$ give sensibly identical results. Table I illustrates, for $r_s < 1$, the maximum relative errors made on σ_e when the exchange and correlation corrections are not taken into account and U_{ex} is replaced by the Lindhard function (U_l) or by the Thomas-Fermi approximation (U_{TF}). In this table σ^{ex}, σ^l, and σ^{TF} correspond, respectively, to U_{ex}, U_l, and U_{TF}.

TABLE I. Maximum relative errors made on σ_e at different temperatures, when U_{ex} is replaced by Thomas-Fermi (U_{TF}) or Lindhard (U_l) functions ($r_s < 1$).

T(K)	10^4	10^5	10^6	10^7	10^8
$(\sigma^{ex}-\sigma^l)/\sigma^{ex}$	+0.02	+0.04	+0.04	+0.02	+0.003
$(\sigma^{ex}-\sigma^{TF})/\sigma^{ex}$	−0.1	−0.07	−0.04	−0.02	−0.006

V. NUMERICAL RESULTS FOR DENSE HYDROGEN PLASMAS

Different conditions imposed by the NFE and OCP models define the boundaries of a region in the $T-r_i$ (or $T-n_i$) plane where both models remain simultaneously valid. This region is shown in Fig. 1. The line $\delta=1$ is due to the fact that in the framework of the OCP model the ions are treated classically. This implies that

$$\delta \equiv \Lambda/r_i \ll 1 \quad \text{or} \quad r_s(Z^{1/3}) \gg 32.87T^{-1/2}, \tag{27}$$

where $\Lambda = (2\pi\hbar^2/M_i k_B T)^{1/2}$ is the thermal de Broglie wavelength. As can be seen from Fig. 1, almost

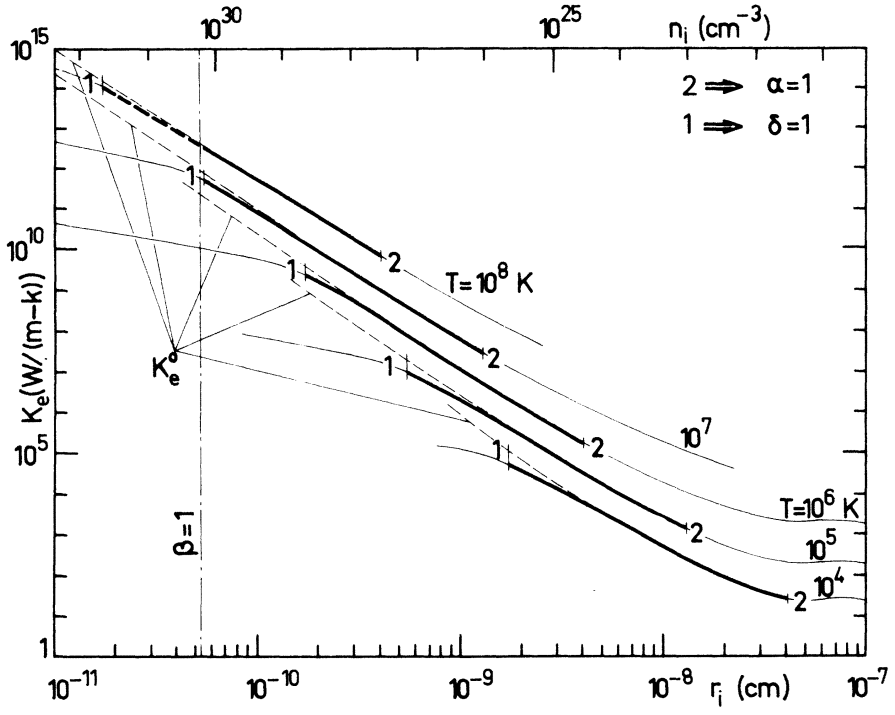

FIG. 4. Electronic thermal conductivity K_e of hydrogen. For comparison, the thermal conductivity K_e^0, derived from the Wiedemann-Franz relation (without taking into account the inelastic electron scattering), is also plotted (dashed curves).

the entire path of a system undergoing changes under the laser-driven fusion regime lies inside this region. The subregions A and B represent, respectively, the initial and the final states of such a system.

The general behavior of the electronic transport coefficients of hydrogen at different densities and temperatures is shown in Figs. 2–8. The elec-

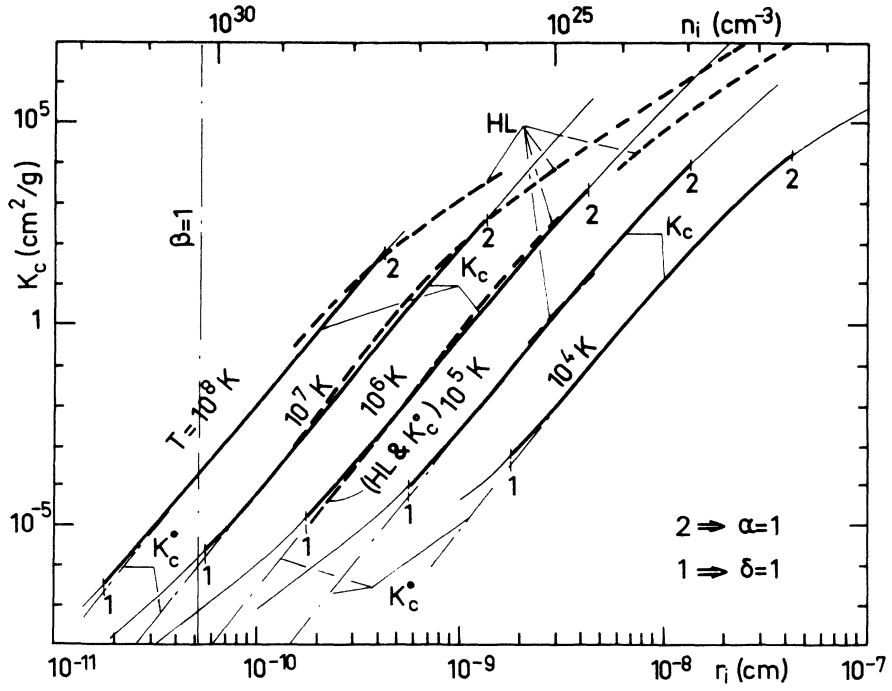

FIG. 5. Conductive opacity K_c of hydrogen. Curve HL: results of Hubbard and Lampe. Curves K_c and K_c^0: our results obtained, respectively, from K_e and K_e^0.

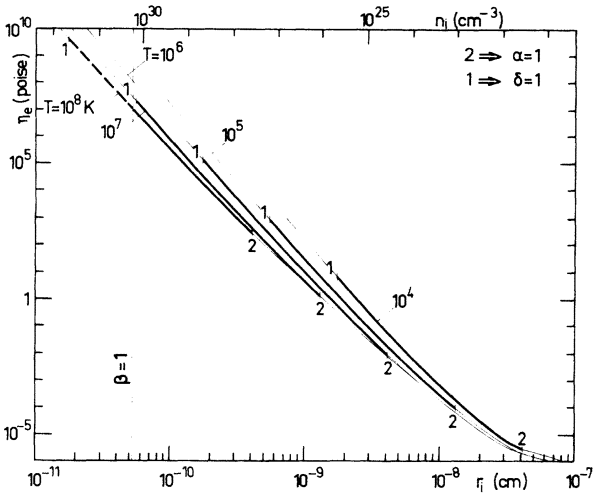

FIG. 6. Electronic bulk viscosity η_e of hydrogen.

trical conductivity was obtained from Eq. (14), the thermal conductivity from (15)–(18), the conductive opacity from (19), the electronic bulk viscosity from (22), and the thermoelectric power from (24) and (25). In these calculations we used $U(k)$ as defined by Eqs. (C3) and (C7) and $S(k)$ of the OCP. In each curve the points 1 and 2 correspond to the conditions $\delta = 1$ and $\alpha = 1$, respectively.

The results of these calculations, are given in Tables II–IV for $T = 10^8$, 10^7, and 10^6 K. For $\Gamma \geq 1$ the structure factor was obtained from the Monte Carlo data, while for $\Gamma < 1$ it was obtained from the hypernetted-chain (HNC) integral equation (Appendix A).

The simple long-wavelength limit of $S(k)$, Eq. (8), was also used to evaluate the transport coefficients of hydrogen at different temperatures and densities. Some of these results are summarized in Tables V and VI for $T = 10^8$ and 10^7 K, respec-

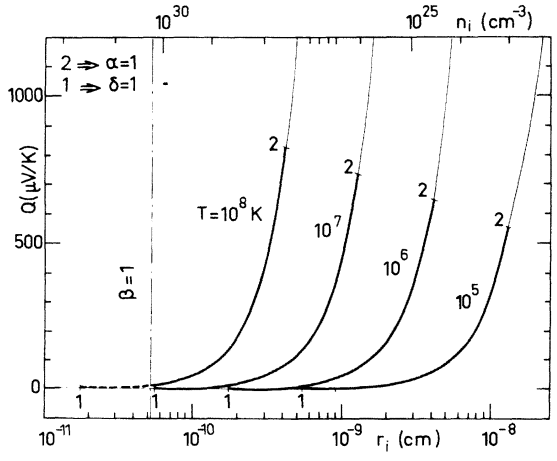

FIG. 7. Thermoelectric power Q of hydrogen.

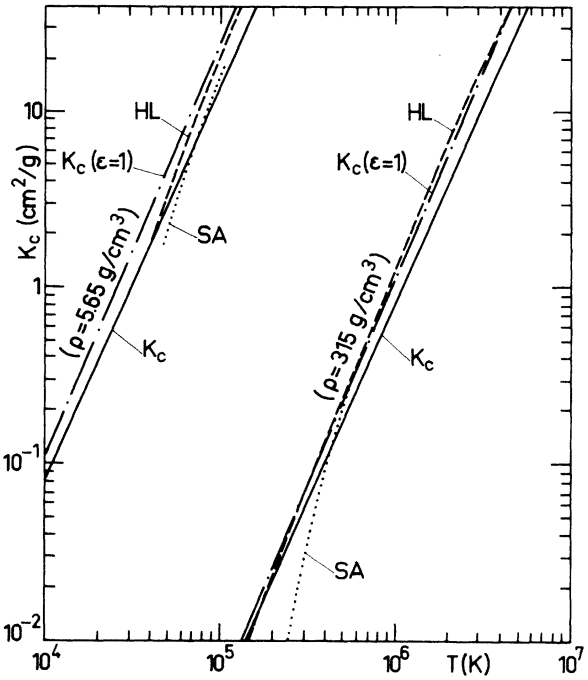

FIG. 8. Conductive opacity of hydrogen at different temperatures and at two densities (ρ). Curves HL: results of Hubbard and Lampe; curve SA: results of Stevenson and Ashcroft; curve K_c: from our results [with Eq. (C 7) for ϵ]; curve K_c ($\epsilon = 1$): our results without the electron screening.

tively. A comparison between the approximate results of these tables and the "exact" values of Tables II and III shows that this approximation is quite satisfactory especially for low values of Γ.

VI. DISCUSSION

In general, the accuracy of the results given in Tables II–IV depends mainly on the accuracy with which $S(k)$ is known. With the more accurate data, based on extensive Monte Carlo runs,[4] it is expected that the overall error of these results should be less than 1%. More specifically, the following remarks, concerning the various transport coefficients, are in order.

1. Electrical conductivity

In the computations relative to σ_e, the effects of inelastic electron scattering from the ionic density fluctuations are not taken into account. In fact, their contribution is negligible in this case.[10]

The condition $\lambda_e / r_i > 1$, pointed out in Sec. II, defines the boundary of a region in the $\sigma_e - r_i$ plane, where the NFE model is applicable. This limit is shown in Figs. 2 and 3 by the line $\lambda_e = r_i$, and as can be seen from these figures our calcula-

TABLE II. Electronic transport coefficients of hydrogen at different densities and at $T = 10^8$ K. σ_e is the electrical conductivity; K_e^0 is the thermal conductivity without the inelastic collision term; K_e is the thermal conductivity with the inelastic collision term; $\alpha_1 = (K_e^0 - K_e)/K_e$; K_c^0 and K_c are the conductive opacities obtained, respectively, from K_e^0 and K_e; η_e is the bulk viscosity; Q is the thermoelectric power. $S(k)$ was obtained from the HNC equation.

Γ	n_i (cm^{-3})	r_i (cm)	σ_e ($\Omega^{-1}\,cm^{-1}$)	K_e^0 ($W\,m^{-1}\,K^{-1}$)	K_e ($W\,m^{-1}\,K^{-1}$)	α_1	K_c^0 ($cm^2\,g^{-1}$)	K_c ($cm^2\,g^{-1}$)	η_e (P)	Q ($\mu V\,K^{-1}$)
0.04	3.274×10^{27}	4.177×10^{-10}	3.250×10^{7}	7.938×10^{9}	7.936×10^{9}	2.650×10^{-4}	69.52	69.54	273.1	819.3
0.05	6.396×10^{27}	3.342×10^{-10}	6.196×10^{7}	1.514×10^{10}	1.513×10^{10}	4.343×10^{-4}	18.67	18.68	808.7	525.7
0.06	1.105×10^{28}	2.785×10^{-10}	1.058×10^{8}	2.585×10^{10}	2.583×10^{10}	6.534×10^{-4}	6.327	6.331	1983	365.5
0.07	1.755×10^{28}	2.387×10^{-10}	1.673×10^{8}	4.086×10^{10}	4.082×10^{10}	9.263×10^{-4}	2.520	2.523	4263	268.7
0.08	2.620×10^{28}	2.089×10^{-10}	2.497×10^{8}	6.099×10^{10}	6.091×10^{10}	1.256×10^{-3}	1.131	1.133	8312	205.7
0.09	3.730×10^{28}	1.857×10^{-10}	3.565×10^{8}	8.709×10^{10}	8.695×10^{10}	1.647×10^{-3}	0.5563	0.5573	1.503×10^{4}	162.5
0.10	5.117×10^{28}	1.671×10^{-10}	4.914×10^{8}	1.200×10^{11}	1.198×10^{11}	2.101×10^{-3}	0.2943	0.2949	2.561×10^{4}	131.6
0.12	8.842×10^{28}	1.392×10^{-10}	8.605×10^{8}	2.102×10^{11}	2.095×10^{11}	3.215×10^{-3}	9.724×10^{-2}	9.756×10^{-2}	6.479×10^{4}	91.25
0.14	1.404×10^{29}	1.194×10^{-10}	1.388×10^{9}	3.391×10^{11}	3.375×10^{11}	4.619×10^{-3}	3.796×10^{-2}	3.814×10^{-2}	1.428×10^{5}	66.94
0.16	2.096×10^{29}	1.044×10^{-10}	2.107×10^{9}	5.148×10^{11}	5.115×10^{11}	6.336×10^{-3}	1.675×10^{-2}	1.686×10^{-2}	2.844×10^{5}	51.16
0.18	2.984×10^{29}	9.283×10^{-11}	3.053×10^{9}	7.457×10^{11}	7.395×10^{11}	8.387×10^{-3}	8.122×10^{-3}	8.190×10^{-3}	5.236×10^{5}	40.35
0.20	4.094×10^{29}	8.355×10^{-11}	4.260×10^{9}	1.041×10^{12}	1.030×10^{12}	1.079×10^{-2}	4.243×10^{-3}	4.289×10^{-3}	9.059×10^{5}	32.63
0.22	5.449×10^{29}	7.595×10^{-11}	5.767×10^{9}	1.409×10^{12}	1.390×10^{12}	1.357×10^{-2}	2.355×10^{-3}	2.387×10^{-3}	1.490×10^{6}	26.91
0.24	7.074×10^{29}	6.962×10^{-11}	7.612×10^{12}	1.859×10^{12}	1.829×10^{12}	1.673×10^{-2}	1.374×10^{-3}	1.397×10^{-3}	2.351×10^{6}	22.58
0.26	8.994×10^{29}	6.427×10^{-11}	9.835×10^{9}	2.402×10^{12}	2.355×10^{12}	2.031×10^{-2}	8.365×10^{-4}	8.535×10^{-4}	3.579×10^{6}	19.20
0.28	1.123×10^{30}	5.968×10^{-11}	1.248×10^{10}	3.048×10^{12}	2.975×10^{12}	2.430×10^{-2}	5.280×10^{-4}	5.408×10^{-4}	5.288×10^{6}	16.53
0.30	1.382×10^{30}	5.570×10^{-11}	1.558×10^{10}	3.806×10^{12}	3.699×10^{12}	2.874×10^{-2}	3.428×10^{-4}	3.536×10^{-4}	7.610×10^{6}	14.37
0.32	1.677×10^{30}	5.222×10^{-11}	1.919×10^{10}	4.687×10^{12}	4.534×10^{12}	3.363×10^{-2}	2.300×10^{-4}	2.377×10^{-4}	1.070×10^{7}	12.61

TABLE III. Electronic transport coefficients at $T = 10^7$ K. $S(k)$ was obtained from the HNC equation for $\Gamma < 1$ and from Monte Carlo data of the OCP for $\Gamma \geq 1$

Γ	n_i (cm^{-3})	r_i (cm)	σ_e ($\Omega^{-1}\,cm^{-1}$)	K_e^0 ($W\,m^{-1}\,K^{-1}$)	K_e ($W\,m^{-1}\,K^{-1}$)	α_1	K_c^0 ($cm^2\,g^{-1}$)	K_c ($cm^2\,g^{-1}$)	η_e (P)	Q ($\mu V\,K^{-1}$)
0.1	5.117×10^{25}	1.671×10^{-9}	8.734×10^{5}	2.133×10^{7}	2.133×10^{7}	1.616×10^{-4}	1656	1656	0.5427	1217
0.2	4.094×10^{26}	8.355×10^{-10}	6.064×10^{6}	1.481×10^{8}	1.480×10^{8}	7.672×10^{-4}	29.81	29.83	14.43	311.3
0.3	1.382×10^{27}	5.570×10^{-10}	2.003×10^{7}	4.893×10^{8}	4.883×10^{8}	1.972×10^{-3}	2.674	2.679	106.4	138.9
0.4	3.275×10^{27}	4.177×10^{-10}	4.798×10^{7}	1.172×10^{9}	1.167×10^{9}	3.912×10^{-3}	0.4709	0.4728	454.0	77.99
0.5	6.396×10^{27}	3.342×10^{-10}	9.574×10^{7}	2.339×10^{9}	2.323×10^{9}	6.711×10^{-3}	0.1208	0.1216	1423	49.75
0.6	1.105×10^{28}	2.785×10^{-10}	1.697×10^{8}	4.146×10^{9}	4.103×10^{9}	1.048×10^{-2}	3.945×10^{-2}	3.986×10^{-2}	3658	34.41
0.7	1.755×10^{28}	2.387×10^{-10}	2.767×10^{8}	6.759×10^{9}	6.657×10^{9}	1.532×10^{-2}	1.523×10^{-2}	1.547×10^{-2}	8180	25.17
0.8	2.620×10^{28}	2.089×10^{-10}	4.241×10^{8}	1.036×10^{10}	1.014×10^{10}	2.134×10^{-2}	6.660×10^{-3}	6.802×10^{-3}	1.650×10^{4}	19.18
0.9	3.730×10^{28}	1.857×10^{-10}	6.194×10^{8}	1.513×10^{10}	1.471×10^{10}	2.861×10^{-2}	3.202×10^{-3}	3.294×10^{-3}	3.074×10^{4}	15.09
1	5.117×10^{28}	1.671×10^{-10}	8.708×10^{8}	2.127×10^{10}	2.051×10^{10}	3.724×10^{-2}	1.661×10^{-3}	1.722×10^{-3}	5.376×10^{4}	12.16
2	4.094×10^{29}	8.355×10^{-11}	8.444×10^{9}	2.063×10^{11}	1.699×10^{11}	0.2139	2.141×10^{-5}	2.598×10^{-5}	2.228×10^{6}	2.912
3	1.382×10^{30}	5.570×10^{-11}	3.282×10^{10}	8.017×10^{11}	4.994×10^{11}	0.6053	1.632×10^{-6}	2.620×10^{-6}	2.058×10^{7}	1.241

TABLE IV. Electronic transport coefficients at $T = 10^6$ K. $S(k)$ was obtained from the HNC equation for $\Gamma < 1$ and from Monte Carlo data of the OCP for $\Gamma \geq 1$.

Γ	n_i (cm^{-3})	r_i (cm)	σ_e ($\Omega^{-1}\,cm^{-1}$)	K_e^0 ($W\,m^{-1}\,K^{-1}$)	K_e ($W\,m^{-1}\,K^{-1}$)	α_1	K_c^0 ($cm^2\,g^{-1}$)	K_c ($cm^2\,g^{-1}$)	η_e (P)	Q ($\mu V\,K^{-1}$)
0.4	3.275×10^{24}	4.177×10^{-9}	9.772×10^{4}	2.387×10^{5}	2.387×10^{5}	2.612×10^{-4}	2312	2313	1.172×10^{-2}	673.0
0.5	6.396×10^{24}	3.342×10^{-9}	1.761×10^{5}	4.302×10^{5}	4.301×10^{5}	4.383×10^{-4}	656.8	657.1	3.223×10^{-2}	439.5
0.6	1.105×10^{25}	2.785×10^{-9}	2.893×10^{5}	7.066×10^{5}	7.061×10^{5}	6.725×10^{-4}	231.4	231.6	7.510×10^{-2}	308.9
0.7	1.755×10^{25}	2.387×10^{-9}	4.444×10^{5}	1.086×10^{6}	1.085×10^{6}	9.697×10^{-4}	94.86	94.95	0.1556	228.6
0.8	2.620×10^{25}	2.089×10^{-9}	6.492×10^{5}	1.586×10^{6}	1.584×10^{6}	1.335×10^{-3}	43.51	43.56	0.2950	175.8
0.9	3.730×10^{25}	1.857×10^{-9}	9.115×10^{5}	2.227×10^{6}	2.223×10^{6}	1.775×10^{-3}	21.76	21.80	0.5224	139.3
1	5.117×10^{25}	1.671×10^{-9}	1.240×10^{6}	3.028×10^{6}	3.021×10^{6}	2.294×10^{-3}	11.66	11.69	0.8753	113.0
2	4.094×10^{26}	8.355×10^{-10}	1.016×10^{7}	2.482×10^{7}	2.451×10^{7}	1.286×10^{-2}	0.1779	0.1802	29.11	27.83
3	1.382×10^{27}	5.570×10^{-10}	3.705×10^{7}	9.051×10^{7}	8.733×10^{7}	3.647×10^{-2}	1.445×10^{-2}	1.498×10^{-2}	246.9	11.98
4	3.275×10^{27}	4.177×10^{-10}	9.358×10^{7}	2.286×10^{8}	2.124×10^{8}	7.630×10^{-2}	2.414×10^{-3}	2.598×10^{-3}	1140	6.542
6	1.105×10^{28}	2.785×10^{-10}	3.539×10^{8}	8.644×10^{8}	7.094×10^{8}	0.2185	1.892×10^{-4}	2.305×10^{-4}	1.026×10^{4}	2.726
10	5.117×10^{28}	1.671×10^{-10}	1.921×10^{9}	4.692×10^{9}	2.576×10^{9}	0.8215	7.528×10^{-6}	1.371×10^{-5}	1.692×10^{5}	0.8653

TABLE V. Electronic transport coefficients at $T=10^8$ K. $S(k)$ was obtained from the theoretical expression at the long-wavelength limit.

Γ	n_i (cm^{-3})	r_i (cm)	σ_e ($\Omega^{-1}\,cm^{-1}$)	K_e^0 ($W\,m^{-1}\,K^{-1}$)	K_e ($W\,m^{-1}\,K^{-1}$)	η_e (P)	Q ($\mu V\,K^{-1}$)
0.04	3.274×10^{27}	4.177×10^{-10}	3.419×10^{7}	8.351×10^{9}	8.349×10^{9}	293.9	814.3
0.05	6.396×10^{27}	3.342×10^{-10}	6.464×10^{7}	1.579×10^{10}	1.578×10^{10}	861.3	523.0
0.06	1.105×10^{28}	2.785×10^{-10}	1.096×10^{8}	2.677×10^{10}	2.675×10^{10}	2094	363.9
0.07	1.755×10^{28}	2.387×10^{-10}	1.721×10^{8}	4.204×10^{10}	4.200×10^{10}	4467	267.7
0.08	2.620×10^{28}	2.089×10^{-10}	2.555×10^{8}	6.241×10^{10}	6.233×10^{10}	8657	205.1
0.09	3.730×10^{28}	1.857×10^{-10}	3.631×10^{8}	8.870×10^{10}	8.855×10^{10}	1.558×10^{4}	162.1
0.10	5.117×10^{28}	1.671×10^{-10}	4.984×10^{8}	1.218×10^{11}	1.215×10^{11}	2.644×10^{4}	131.3
0.12	8.842×10^{28}	1.392×10^{-10}	8.668×10^{8}	2.117×10^{11}	2.111×10^{11}	6.648×10^{4}	91.07
0.14	1.404×10^{29}	1.194×10^{-10}	1.391×10^{9}	3.397×10^{11}	3.382×10^{11}	1.459×10^{5}	66.83
0.16	2.096×10^{29}	1.044×10^{-10}	2.102×10^{9}	5.135×10^{11}	5.103×10^{11}	2.898×10^{5}	51.09
0.18	2.984×10^{29}	9.283×10^{-11}	3.034×10^{9}	7.411×10^{11}	7.350×10^{11}	5.328×10^{5}	40.30
0.20	4.094×10^{29}	8.355×10^{-11}	4.221×10^{9}	1.031×10^{12}	1.020×10^{12}	9.211×10^{5}	32.59
0.22	5.449×10^{29}	7.595×10^{-11}	5.698×10^{9}	1.392×10^{12}	1.374×10^{12}	1.515×10^{6}	26.88
0.24	7.074×10^{29}	6.962×10^{-11}	7.503×10^{9}	1.833×10^{12}	1.803×10^{12}	2.390×10^{6}	22.55
0.26	8.994×10^{29}	6.427×10^{-11}	9.673×10^{9}	2.363×10^{12}	2.317×10^{12}	3.642×10^{6}	19.18
0.28	1.123×10^{30}	5.968×10^{-11}	1.225×10^{10}	2.992×10^{12}	2.922×10^{12}	5.384×10^{6}	16.50
0.30	1.382×10^{30}	5.570×10^{-11}	1.527×10^{10}	3.729×10^{12}	3.627×10^{12}	7.757×10^{6}	14.35
0.32	1.677×10^{30}	5.222×10^{-11}	1.877×10^{10}	4.585×10^{12}	4.439×10^{12}	1.093×10^{7}	12.59

tions are well within the region of validity of the NFE model.

2. *Thermal conductivity and conductive opacity*

The inclusion of the inelastic electron scattering effects introduces non-negligible corrections to the electronic thermal conductivity and hence to the conductive opacity (see Tables II–VI). A comparison is made between K_e (solid curves) and K_e^0 (dashed curves) in Fig. 4, where K_e^0 is obtained from the Wiedemann-Franz relation (15) and K_e from expresssions (17) and (18). The factor α_1, given by expression (18), represents the deviation of the Lorenz number from the ideal Sommerfeld value, due to the inelastic electron scattering effects. As can be seen from the values of α_1 given in Tables II–IV, the contribution to K_e from the inelastic scattering of electrons becomes important at higher densities and lower temperatures.

In Figs. 5 and 8, our results for the conductive opacity are compared with those given by Hubbard and Lampe (HL).[7] K_c and K_c^0 are computed, respectively, from K_e and K_e^0 using expression (19). Our results, in the region of applicability of the NFE-OCP models, should be more accurate than those of HL for the following reasons:

(a) The values that we are using for the structure factor are much more accurate than those used by HL.

(b) The screening effect of the electrons is included explicitly in our calculations. In fact, the important contribution of the electron screening is illustrated in Fig. 8, where the curves K_c and

TABLE VI. Electronic transport coefficients at $T=10^7$ K. $S(k)$ was obtained from the theoretical expression at the long-wavelength limit.

Γ	n_i (cm^{-3})	r_i (cm)	σ_e ($\Omega^{-1}\,cm^{-1}$)	K_e^0 ($W\,m^{-1}\,K^{-1}$)	K_e ($W\,m^{-1}\,K^{-1}$)	η_e (P)	Q ($\mu V\,K^{-1}$)
0.1	5.117×10^{25}	1.671×10^{-9}	8.707×10^{5}	2.127×10^{7}	2.127×10^{7}	0.5485	1215
0.2	4.094×10^{26}	8.355×10^{-10}	6.000×10^{6}	1.466×10^{8}	1.465×10^{8}	14.71	310.8
0.3	1.382×10^{27}	5.570×10^{-10}	1.969×10^{7}	4.809×10^{8}	4.800×10^{8}	109.6	138.5
0.4	3.275×10^{27}	4.177×10^{-10}	4.687×10^{7}	1.145×10^{9}	1.141×10^{9}	472.7	77.69
0.5	6.396×10^{27}	3.342×10^{-10}	9.298×10^{7}	2.271×10^{9}	2.257×10^{9}	1499	49.49
0.6	1.105×10^{28}	2.785×10^{-10}	1.639×10^{8}	4.003×10^{9}	3.963×10^{9}	3894	34.17
0.7	1.755×10^{28}	2.387×10^{-10}	2.657×10^{8}	6.491×10^{9}	6.397×10^{9}	8804	24.95
0.8	2.620×10^{28}	2.089×10^{-10}	4.050×10^{8}	9.894×10^{9}	9.696×10^{9}	1.795×10^{4}	18.97
0.9	3.730×10^{28}	1.857×10^{-10}	5.885×10^{8}	1.437×10^{10}	1.399×10^{10}	3.380×10^{4}	14.89
1	5.117×10^{28}	1.671×10^{-10}	8.229×10^{8}	2.010×10^{10}	1.942×10^{10}	5.973×10^{4}	11.98
2	4.094×10^{29}	8.355×10^{-11}	7.537×10^{9}	1.841×10^{11}	1.546×10^{11}	2.718×10^{6}	2.766
3	1.382×10^{30}	5.570×10^{-11}	2.690×10^{10}	6.571×10^{11}	4.392×10^{11}	2.669×10^{7}	1.107

K_c ($\epsilon = 1$) represent our results using the OCP structure factor. The curves K_c are computed with $U(k)$ from expression (C3) combined with (C5) and (C7) for the dielectric function, while the curves K_c ($\epsilon = 1$) are obtained by putting $\epsilon(k) = 1$ in (C3) for $U(k)$ and hence disregarding the electron screening. Although in Ref. 7 the expression used for the scattering potential in the region of interest is not given explicitly, it seems that in this region the HL computations are based mainly on a previous work by Hubbard, where an expression analogous to (C3) with $\epsilon(k) = 1$ was used [see Ref. 8, Eq. (19)].

(c) As was stated above, we include in our calculations the effects of inelastic electron scattering from the ionic density fluctuations.

The results given by Stevenson and Ashcroft[3] (SA) for the conductive opacity are also included in Fig. 8. The discrepancy between the SA results and ours might be attributed to the uncertainties of the temperature dependence of the hard-sphere model, as was discussed in Sec. IV and illustrated in Fig. 2 for the electrical conductivity.

APPENDIX A: STRUCTURE FACTOR OF THE OCP

The excess thermodynamic properties and the equilibrium distribution functions of the classical one-component plasma depend only on the dimensionless parameter

$$\Gamma = \beta(Ze)^2/r_i \ ,$$

where r_i is the ion sphere radius. In Ref. 4 the pair distribution function $g(r)$ was calculated "exactly" in the range $1 \leq \Gamma \leq 160$ by the Monte Carlo method. The structure factor is then immediately obtained by the Fourier transform

$$S(q) = 1 + 3\int_0^\infty [g(X) - 1]\,\frac{\sin qX}{qX}\,X^2\,dX \ , \qquad \text{(A1)}$$

where $q = kr_i$ and $X = r/r_i$. However, since the simulated systems are of finite size (a few hundred particles in a cubic volume, with periodic boundary conditions), $g(X)$ is known only in the range $X \leq \frac{1}{2}L$, where L is the cube edge (L is typically of the order of 5). At large values of Γ, $g(X)$ has pronounced oscillations which are not yet sufficiently damped for $X = \frac{1}{2}L$, so that large truncation errors occur in the evaluation of (A1). Consequently an extrapolation scheme is needed to obtain accurate values of $g(X)$ in the range $X > \frac{1}{2}L$. We have used a method inspired by a similar scheme devised by Verlet[17] in the study of classical liquids. $g(X)$ is obtained for $X > \frac{1}{2}L$ by solving the set of equations

$$g(X) = g_{\mathrm{MC}}(X), \quad X \leq \tfrac{1}{2}L \ , \qquad \text{(A2)}$$

$$C(X) = -\Gamma/X, \quad X > \tfrac{1}{2}L \ , \qquad \text{(A3)}$$

complemented by the Ornstein-Zernike relation between $g(X)$ and $C(X)$,

$$g(X) - 1 = C(X) + \frac{3}{4\pi}\int [g(X') - 1]\,C(|\vec{\mathrm{X}} - \vec{\mathrm{X}}'|)\,d\vec{\mathrm{X}}' \ . \qquad \text{(A4)}$$

Here $C(X)$ is the direct correlation function, and $g_{\mathrm{MC}}(X)$ denotes the pair distribution function calculated by the Monte Carlo method for $X \leq \frac{1}{2}L$. Note that $n_i r_i^3 = 3/4\pi$. Equations (A2)–(A4) form a closed set which can be solved iteratively like the usual integral equations. The ansatz (A3) is justified by the fact that in the OCP $C(X)$ tends rapidly towards its Debye-Hückel limit $-\beta(Ze)^2/r = -\Gamma/X$, for all values of Γ. The Monte Carlo calculations have shown that $C(X)$ differs from $-\Gamma/X$ by less than 1% at a distance of the order of the mean inter-ionic spacing ($X \simeq 1.6$). For $X \simeq \frac{1}{2}L$ the difference between $C(X)$ and its asymptotic form is completely negligible, so that the ansatz (A3) is practically exact. $S(q)$ as determined by this method is tabulated for several values of Γ elsewhere.[18]

For $\Gamma \lesssim 1$ the structure factor can be calculated quite accurately by solving the HNC integral equation.[19]

In the range $q \lesssim 2$, $S(q)$ is everywhere very close to its exact long-wavelength limit given by (8).[11]

APPENDIX B: STRUCTURE FACTOR FROM THE HARD-SPHERE MODEL

The integral equation of Percus and Yevick for the pair distribution function has an exact solution for the special case of the hard-sphere model.[20,21]

The structure factor is obtained[16] in the form

$$[S(u)]^{-1} = 1 + F(u)[\sin u\, f(u) + \cos u\, g(u) + h(u)] \ , \qquad \text{(B1)}$$

where the dimensionless variable u is connected to the hard-sphere radius r_h by the relation $u = 2kr_h$. As a function of the parameters x and p defined by $x \equiv k/2k_F$ and $p \equiv r_h/r_i$, the variable u can be expressed as

$$u = (144\pi Z)^{1/3} p x \ . \qquad \text{(B2)}$$

The functions $F(u)$, $f(u)$, $g(u)$, and $h(u)$ in formula (B1) are

$$F(u) = 24(p/u^2)^3 \ ,$$

$$f(u) = u[u^2(\alpha + 2\beta + 4\gamma) - 24\gamma] \ ,$$

$$g(u) = -u^4(\alpha + \beta + \gamma) + 2u^2(\beta + 6\gamma) - 24\gamma \ ,$$

$$h(u) = -2\beta u^2 + 24\gamma \ ,$$

and α, β, and γ are different functions of p,

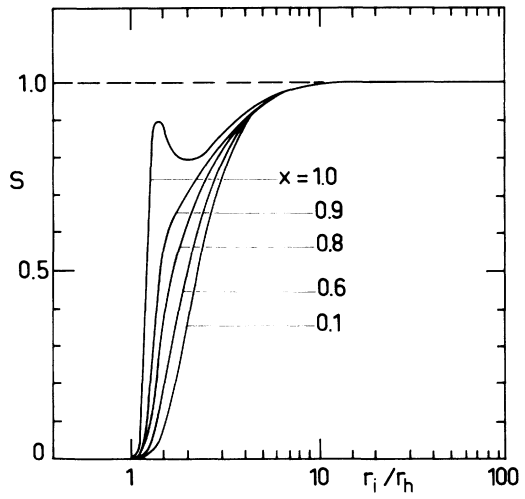

FIG. 9. Values of the hard-sphere structure factor for five values of $x = k/2k_F$, as a function of $r_i = (\frac{4}{3}\pi n_i)^{-1/3}$.

$$\alpha = (1+2p^3)^2/(1-p^3)^4 ,$$

$$\beta = -6p^3(1+\tfrac{1}{2}p^3)^2/(1-p^3)^4 ,$$

$$\gamma = \tfrac{1}{2}p^3(1+2p^3)^2/(1-p^3)^4 .$$

Figure 9 gives as a function of p^{-1} the behavior of the structure factor for five values of $x = k/2k_F$, as calculated from formula (B1) with u given by (B2). It can be seen from these calculations that

$$S(x) \geq 0.992 ,$$

when $r_i \geq 10r_h$ and $0 \leq x \leq 1$, and

$$S(x) \to 0 ,$$

when $r_i \to r_h$, so that in the transport coefficients given in Sec. III the structure factor obtained from the hard-sphere model has a contribution in the density range defined by

$$1 < r_i/r_h < 10 . \tag{B3}$$

APPENDIX C: SCATTERING POTENTIAL AND DIELECTRIC FUNCTION

In the simplest form the screened Coulomb potential around a point ion, as first given by Mott, is

$$V = -(Ze^2/r)e^{-q_{TF}r} \tag{C1}$$

where $q_{TF} = (4k_F/\pi a_0)^{1/2}$ is the inverse of the Thomas-Fermi screening length. In the Thomas-Fermi approximation, $U(k)$ is taken as the Fourier transform of this potential,

$$U(k) = -\tfrac{4}{3}k_F^3 e^2/\pi(k^2 + q_{TF}^2) , \tag{C2}$$

or in the alternative form

$$U(k) = U_0/\epsilon(k) , \tag{C3}$$

where $U_0 = -4\pi n_e e^2/k^2$ and the dielectric function $\epsilon(k)$ is given by

$$\epsilon(k) = (k^2 + q_{TF}^2)/k^2 . \tag{C4}$$

A more accurate form of $\epsilon(k)$ is obtained in the framework of the random phase approximation by Lindhard and Bardeen. Their result is[22]

$$\epsilon(k) = [k^2 + q_{TF}^2 f(k/2k_F)]/k^2 , \tag{C5}$$

$$f(x) = \frac{1}{2} + \frac{x^2-1}{4x}\ln\left|\frac{1-x}{1+x}\right| , \tag{C6}$$

This expression is valid rigorously only in a very-high-density Fermi gas, when $r_s \ll 1$. At the lower densities the exchange and correlation corrections should be taken into account. This leads to another expression for $\epsilon(k)$ similar to the expression (C5), where the Lindhard function $f(x)$ is replaced here by[23]

$$F(x) = \frac{f(x)}{1 - (q_{TF}/2k_F)^2 f(x)(2x^2+g)^{-1}} , \tag{C7}$$

where

$$g = (1 + 0.0262r_s)^{-1} .$$

APPENDIX D: CHESTER-THELLUNG-HUBBARD FORMALISM

We follow closely the Hubbard presentation[8] of the Chester-Thellung version[9] of the Kubo formalism for the linear response theory.

The time-independent transport coefficients G_{ij} of the electron gas are isotropic tensors defined by

$$\vec{J} = eG_{11}(e\vec{E}) + eG_{12}(\vec{\nabla}T)/T , \tag{D1}$$

$$\vec{Q} = -G_{21}(e\vec{E}) - G_{22}(\vec{\nabla}T)/T , \tag{D2}$$

where $\vec{J}$ is the electric current density, $\vec{Q}$ is the electron energy crossing unit area per unit time, and $\vec{E}$ is the electric field.

In the following, we shall restrict ourselves to S_{ij} which are the diagonal parts of the tensors G_{ij}. The electron thermal conductivity is then explicitly given by

$$K_e = (S_{11}S_{22} - S_{12}S_{21})/TS_{11} , \tag{D3}$$

so that $\vec{Q} = -K_e\vec{\nabla}T$ when $\vec{J} = 0$.

In the Lorentz model, the single-electron Hamiltonian reads

$$H = \frac{p^2}{2m_e} - \sum_{\alpha=1}^{N_i} e^2\left|\vec{r} - \vec{r}_\alpha\right|^{-1} , \tag{D4}$$

where the sum is taken over all of the N_i protons located at $\vec{r}_\alpha$. $\vec{p}$ and $\vec{r}$ are the momentum and position operators of an electron. K_e is now evaluated with the weak-coupling approximation, such that

the H eigenstates may be taken as plane waves for independent electrons diagonalizing the kinetic term.

Chester and Thellung[9] have shown that the Kubo expressions for the G_{ij} may then be obtained from the generating function

$$\mathcal{L}(y)=\sum_s\sum_{s'}\left(\frac{-1}{m_e^2V}\right)\int\frac{Vd^3p}{(2\pi\hbar)^3}\int\frac{Vd^3p'}{(2\pi\hbar)^3}\frac{\partial f}{\partial E}e^{-yE}\vec{p}\vec{p}'\int_0^\infty dtP_t(\vec{p}',s',\vec{p},s)\,, \tag{D5}$$

where $E=p^2/2m_e$. The sums run over spin states. $f=(1+e^{\beta(E-\mu)})^{-1}$ is the Fermi distribution. $P_t(\vec{p}',s',\vec{p},s)$ denotes the probability at time t that an electron is in state $|\vec{p}',s'\rangle$, given that an electron was placed in state $|\vec{p},s\rangle$ at $t=0$. It is obtained as a solution of the master equation

$$\frac{d}{dt}P_t(\vec{p}',s',\vec{p},s)=\sum_{s''}\int\frac{Vd^3p''}{(2\pi\hbar)^3}W(\vec{p}',s',\vec{p}'',s'')P_t(\vec{p}'',s'',\vec{p},s)$$

$$-P_t(\vec{p}',s',\vec{p},s)\sum_{s''}\int\frac{Vd^3p''}{(2\pi\hbar)^3}W(\vec{p}'',s'',\vec{p}',s')\,, \tag{D6}$$

with $W(\vec{p}',s',\vec{p}'',s'')$ the transition probability per unit time for an electron to change from $|\vec{p}'',s''\rangle$ to $|\vec{p}',s'\rangle$. The G_{ij} are then given as

$$G_{11}=\mathcal{L}(0),\qquad G_{12}=G_{21}=-\left.\frac{d\mathcal{L}(y)}{dy}\right|_{y=0},\qquad G_{22}=\left.\frac{d^2\mathcal{L}(y)}{dy^2}\right|_{y=0}. \tag{D7}$$

Integrating Eq. (D6) over time gives

$$-(2\pi\hbar)^3\delta(\vec{p}'-\vec{p})\delta_{ss'}V^{-1}=\sum_{s''}\int\frac{Vd^3p''}{(2\pi\hbar)^3}W(\vec{p}',s',\vec{p}'',s'')I(\vec{p}'',s'',\vec{p},s)$$

$$-I(\vec{p}',s',\vec{p},s)\sum_{s''}\int\frac{Vd^3p''}{(2\pi\hbar)^3}W(\vec{p}'',s'',\vec{p}',s')\,, \tag{D8}$$

where

$$I(\vec{p}',s',\vec{p},s)=\int_0^\infty dtP_t(\vec{p}',s',\vec{p},s)\,,$$

with

$$P_{t=\infty}=0,\quad P_{t=0}=(2\pi\hbar)^3\delta(\vec{p}'-\vec{p})\delta_{ss'}V^{-1}\,.$$

The electron-ion interaction

$$\phi=-\sum_{\alpha=1}^{N_i}e^2|\vec{r}-\vec{r}_\alpha|^{-1}$$

taken in the first Born approximation (weak-coupling) yields the probability

$$W=|\langle\vec{p}',s'|\phi|\vec{p},s\rangle|^2(2\pi m_e/\hbar p)\delta(\vec{p}'-\vec{p})$$

$$=2\pi m_e\frac{\delta(\vec{p}'-\vec{p})}{\hbar pV^2}(4\pi e^2)^2\frac{\delta_{ss'}}{k^4}\sum_{\alpha=1}^{N_i}\sum_{\alpha'=1}^{N_i}e^{i\vec{k}\cdot(\vec{r}_\alpha-\vec{r}_{\alpha'})}\,,$$

with $\vec{k}=(\vec{p}'-\vec{p})\hbar^{-1}$, and the corresponding canonical average

$$\langle W(\vec{p}',s',\vec{p},s)\rangle=2\pi m_e\delta_{ss'}\frac{(4\pi e^2)^2}{k^4}\frac{\delta(\vec{p}'-\vec{p})}{\hbar pV^2}N_iS(k)\,,$$

where

$$S(k)=1+N_ih(k)$$

$$h(k)=V^{-1}\int d^3r\,g(r)e^{i\vec{k}\cdot\vec{r}}\,,$$

in terms of the equilibrium ionic pair distribution function. The above average is meaningful as long as the electron mean free path remains much larger than the mean ionic correlation distance. Thus we may look for a solution of Eq. (D8) in the form

$$I(\vec{p}',s',\vec{p},s)=\delta(\vec{p}'-\vec{p})\,\delta_{ss'}\sum_{l=0}^{\infty}A_l(p)P_l(\xi)\,, \tag{D9}$$

where $\xi=(\vec{p}\cdot\vec{p}')/p^2$ and $P_l(\xi)$ is the Legendre polynomial. Only the $l=1$ term is expected to survive the angular quadrature in Eq. (D5). Inserting Eq. (D9) into (D8) and using

$$\delta(\vec{p}'-\vec{p})=\frac{\delta(\vec{p}'-\vec{p})}{4\pi p^2}\sum_{\alpha=0}^{\infty}(2l+1)P_l(\xi)\,,$$

we get

$$A_1(p)=\frac{3(2\pi\hbar)^3p}{8\pi^2m_e e^4N_i}\left(\int_{-1}^{1}\frac{d\xi\,S(k)}{1-\xi}\right)^{-1}.$$

Measuring momenta in units of r_i^{-1}, we obtain the dimensionless momentum $q=kr_i$, with $1-\xi=\hbar^2q^2/2r_i^2p^2$. The transport generating function becomes

$$\mathcal{L}(y)=-\frac{8\hbar^3n_i}{27\pi m_e^2e^4}J$$

$$\times\int_0^\infty dq\,q^6\frac{\partial f}{\partial q}G(q)\exp\left(\frac{-\hbar^2q^2y}{2r_i^2m_e}\right), \tag{D10}$$

where $n_i = N_i/V$, J is the unit tensor, and

$$G(q)^{-1} = 2\int_0^{2q} dq' \frac{S(q')}{q'} = \frac{1}{\alpha} \ln\left(1 + \frac{4\alpha q^2}{3\Gamma}\right), \quad \text{(D11)}$$

where the "hydrodynamic" structure factor [Eq. (8) in the main text] was used. Specializing Eq. (D10) to completely degenerate electrons and restricting to the first term in the $\partial f/\partial q$ expansion, we obtain

$$\begin{aligned} S_{11} &\sim C_1 q_F^6 G(q_F), \\ S_{12} = S_{21} &\sim C_1 C_3 q_F^8 G(q_F), \\ S_{22} &\sim C_1 C_3^2 q_F^{10} G(q_F), \end{aligned} \quad \text{(D12)}$$

with

$$\begin{aligned} C_1 &= (2\pi\hbar)^3 n_i / 27\pi^4 m_e^2 e^4, \\ 6C_2 &= (m_e k_B T/\hbar^2)^2 (2n_i)^{-4/3}, \\ C_3 &= \hbar^2/2m_e r_i^2. \end{aligned}$$

Equation (D3) is therefore given as

$$K_e = [(2\pi\hbar)^3 k_B^2 / 16 m_e^2 e^4] G(q_F) n_i T,$$

which is nothing but the Boltzmann-Ziman equation (9) in the main text.

---

*Laboratoire associé au CNRS.
†Equipe associée au CNRS.

[1]J. M. Ziman, Philos. Mag. 6, 1013 (1961).
[2]C. Deutsch, J. Non-Cryst. Solids 8-10, 713 (1972).
[3]D. J. Stevenson and N. W. Ashcroft, Phys. Rev. A 9, 782 (1974).
[4]J. P. Hansen, Phys. Rev. A 8, 3096 (1973).
[5]H. Brysk, P. M. Campbell, and P. Hammerling, Plasma Phys. 17, 473 (1975).
[6]M. Lampe, Phys. Rev. 170, 306 (1968); 174, 276 (1968).
[7]W. B. Hubbard and M. Lampe, Astrophys. J. Suppl. 18, 297 (1969).
[8]W. B. Hubbard, Astrophys. J. 3, 858 (1966).
[9]G. V. Chester and A. Thellung, Proc. Phys. Soc. London 77, 1005 (1961).
[10]M. J. Rice, Phys. Rev. B 2, 4800 (1970).
[11]P. Viellefosse and J. P. Hansen, Phys. Rev. A 12, 1106 (1975).
[12]R. Kubo (private communication).
[13]I. Iben, Jr., Astrophys. J. 154, 557 (1968).
[14]G. Baym, Phys. Rev. 135, A1691 (1964).
[15]T. E. Faber, *An Introduction to the Theory of Liquid Metals* (Cambridge U.P., Cambridge, 1972).
[16]N. W. Ashcroft and J. Lekner, Phys. Rev. 145, 83 (1966).
[17]L. Verlet, Phys. Rev. 165, 201 (1968).
[18]S. Galam and J. P. Hansen, this issue, Phys. Rev. A 14, 816 (1976).
[19]J. F. Springer, M. A. Pokrant, and F. A. Stevens, Jr., J. Chem. Phys. 58, 4863 (1973).
[20]M. S. Wertheim, Phys. Rev. Lett. 10, 321 (1963).
[21]E. Thiele, J. Chem. Phys. 39, 474 (1963).
[22]N. H. March, *Liquid Metals* (Pergamon, New York, 1968).
[23]D. J. W. Geldart and S. H. Vosko, Can. J. Phys. 44, 2137 (1966).